Size Discrimination of Carbohydrates via Conductive Carbon Nanotube@Metal Organic Framework Composites

*David L. White,[†] Brian A. Day,[‡] Zidao Zeng,[†] Zachary M. Schulte,[†] Noah R. Borland,[†] Nathaniel L. Rosi,[†,‡] Christopher E. Wilmer,[‡,§] and Alexander Star[†,‖,]**

[†]Department of Chemistry, University of Pittsburgh, Pittsburgh, Pennsylvania, 15260, USA

[‡]Department of Chemical & Petroleum Engineering, University of Pittsburgh, Pittsburgh, Pennsylvania 15260, USA

[§]Department of Electrical & Computer Engineering, University of Pittsburgh, Pittsburgh, Pennsylvania 15260, USA

[‖]Department of Bioengineering, University of Pittsburgh, Pittsburgh, Pennsylvania 15260, USA

Keywords: Metal Organic Frameworks, Carbon Nanotubes, Field-Effect Transistor, Sensors, Molecular Dynamics

Abstract:

Traditional chemical sensing methodologies have typically relied on specific chemistry of the analyte for detection. Modifications to the local environment surrounding the sensor represent an alternative pathway to impart selective differentiation. Here we present the hybridization of a 2-D metal organic framework ($Cu_3(HHTP)_2$) with single-walled carbon nanotubes (SWCNTs) as a methodology for size discrimination of carbohydrates. Synthesis and resulting conductive performance are modulated by both mass loading of SWCNTs and their relative oxidation. Liquid gated field-effect transistor (FET) devices demonstrate improved

on/off characteristics and differentiation of carbohydrates based on molecular size. Glucose molecule detection is limited to the single micromolar concentration range. Molecular Dynamics (MD) calculations on model systems revealed decreases in ion diffusivity in the presence of different sugars as well as packing differences based on the size of a given carbohydrate molecule. The proposed sensing mechanism is a reduction in gate capacitance initiated by the filling of the pores with carbohydrate molecules. Restricting diffusion around a sensor in combination with FET measurements represents a new type of sensing mechanism for chemically similar analytes.

Introduction:

Sensing methodologies utilizing electrical conductivity as a transducing element are well developed technologies with extensive examples in gas phase,[1-5] liquid phase,[6-10] and biological sensing.[11-13] Changes are typically recorded through direct alteration of charge carrier number,[14, 15] modification of local chemical potential,[16] or alteration in local capacitance.[17, 18] Broad improvement in each of these sensing methodologies has been achieved through integration with single-walled carbon nanotubes (SWCNTs). SWCNTs are particularly well-suited to these techniques due to large surface to volume ratios,[19] superior electrical conductivity,[20] and potential semiconducting band structure.[21] The advantages of SWCNTs also typically include other sensitizing chemistry to improve their selectivity.[14, 22] However, most of these techniques degrade the performance of the nanotubes through covalent modification,[23, 24] which limits electrical properties through the generation of trap states. Non-covalent functionalization with polymers[25, 26] can also induce selectivity but limit access the surface of the nanotube, the most sensitive part of the device. Covalent and non-covalent modifications of nanotubes are also limited in identifying

a particular functional group or chemical feature (i.e., electron donating, electron withdrawing, or polar).

Additional limitations of SWCNTs include the inherent heterogeneity present from synthesis. While there have been substantial efforts to improve the chirality of synthesized SWCNTs, such methods typically require substantial post-synthetic effort. A common strategy to generate single chirality SWCNTs is the use of surfactant which preferentially bind one chirality over others. These surfactants are challenging to remove in most cases and inhibit access to the surface of the nanotubes for further synthesis or limiting sensing behavior. Other limitations can include establishing length and diameter control and the relative ratios of semiconducting to metallic nanotubes which affect overall electrical device performance. This work is aimed at commercially available SWCNTs with minimal post synthetic procedures beyond suspension in solvent to establish the broadest potential nature of composite formation.

A relatively less explored area has been the rational integration of metal organic frameworks (MOF) as selective chemical layers for SWCNT-based sensors.[27] The large structural diversity of MOFs allows limitless possibilities to dictate interactions at the surface of sensors.[28] A particular advantage of MOFs over existing covalent chemistry on nanotubes is the wide variety of ways to control morphology of the composite through functional groups present on the nanotube and synthetic conditions. The principal advantage of MOFs when combined with non-covalent functionalization is the retention of access to the surface of nanotubes through the intrinsic porous structure of the MOF. Beyond improvement of sensing performance, SWCNTs provide natural structure to transmit information regarding local chemical events in the pores of the MOFs across long distances through conductivity. While electrically conductive MOFs are a rapidly growing field,[29-34] incorporating SWCNTs into MOFs provides an alternative framework to improve

conductivity with minimal pore disruption, or to make nonconductive frameworks inherit additional properties.

MOFs have been used extensively for sensing without additional materials. Impressive demonstrations of leveraging the tunable structure of the pores have been utilized to yield chiral sensing.[35] Chemiresistive sensing with MOFs have numerous examples for analytes like NH_3,[36] C_6H_6,[37] and volatile organic compounds (VOCs).[38] MOFs also see use in a wide array of electronic applications beyond sensing as well.[39]

Substantial work has been conducted to incorporate MOFs with SWCNTs for a variety of applications. Previous efforts from our group have demonstrated enhanced selective gas sensing of ethanol and DMMP with ZIF-8/SWCNT[27] and UiO-66-NH_2/SWCNT[40] composites, respectively. SWCNT composites with HKUST-1 have shown increased uptake of CO_2[41] or H_2.[42] SWCNTs have been leveraged in composites for lithium ion battery anodes.[43] SWCNTs have also been incorporated into foldable lithium sulfur batteries.[44]

Several composites using multiwalled carbon nanotubes (MWCNT) have also been made for applications in water remediation.[45, 46] Both traditional electrochemical sensing applications[47] as well as electrocatalytic materials for OER/ORR[48]/HER[49] have been realized. Chemiresistive sensing for common VOCs have been another common target for this class of materials.[50, 51] Gas storage and separation for CO_2[52, 53] and H_2[54-56] have been another area of study. Other energy storage applications including supercapacitors have seen initial exploration.[57] There have also been efforts to incorporate graphene sheets into MOFs. Graphene oxide has been used as a structure directing agent to form a single crystal MOF.[58] Graphene has been integrated with MOFs for broadband photodetectors.[59]

SWCNTs are particularly advantageous for this class of material composites for several reasons. Many other conductive MOF composites depend on the presence of molecules, polymers, or 2-D sheets to impart conductivity. In all of those cases, the presence of the conductive component will limit porosity of the MOF. One of the principal advantages, SWCNTs add conductivity through the inclusion of 1-D conductive materials with minimal distribution of porosity as demonstrated by the BET and FTIR results. Another advantage of SWCNTs is the rich suite of chemistry that has been developed to introduce functional groups on the surface of carbon nanotubes. These can interact with wide diversity of MOF linker chemistries to dictate the interface between the materials. SWCNTs also possess an inherent surface for pi to pi stacking. Many MOFs are based on flat aromatic units which enable strong interaction with that pi surface. Conductive molecules and polymers are particularly sensitive to change in their local chemistry which imposes stronger matching conditions for pairing a conductive molecule or polymer with a particular MOF. SWCNTs on the other hand can act as a platform for a wide array of chemistries.

Here we develop a methodology to discriminate chemically similar molecules (i.e., a homologous series of carbohydrates) based only by size. By rationally integrating an existing conductive water stable MOF, copper hexahydroxytriphenylene ($Cu_3(HHTP)_2$),[30] with SWCNTs, we demonstrate changes in field-effect transistor (FET) sensors based on the composites that correlate with a filling of the pores of the $Cu_3(HHTP)_2$. Differential growth of $Cu_3(HHTP)_2$ on unoxidized versus oxidized nanotubes (ox-SWCNTs) is observed, as well as a dependence on electrical conductivity correlated with mass loading of SWCNTs. As the size of the carbohydrate molecule is reduced larger and larger decreases in current can be observed because of decreased gate capacitance. For the smallest sugar molecule, glucose, we observed concentration dependent

decreases in conductance at the most negative applied gate voltage with limits of detection in the single digit micromolar concentration range.

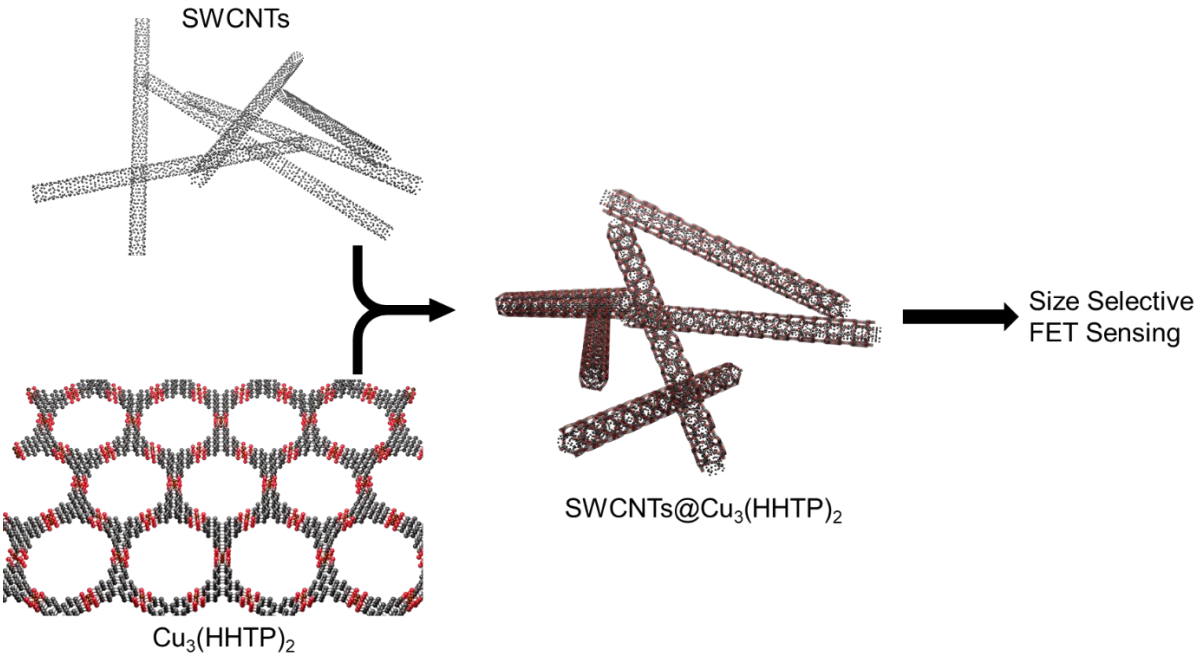

Scheme 1: Illustration of the synthetic strategy utilized to achieve size selective sensing through synergy between $Cu_3(HHTP)_2$ and SWCNTs.

Results and Discussion:

We synthesized $Cu_3(HHTP)_2$ in a solvothermal mixture of water and dimethylformamide (DMF) by slightly modifying the previously reported procedure.[60] DMF was used as the solvent to suspend the nanotubes due to the favorable matching of surface energies.[61] Both unoxidized (SWCNTs) and oxidized (ox-SWCNTs) single-walled carbon nanotubes were used to pursue functional composites. Our previous work had centered primarily around ox-SWCNTs due to the presence of carboxylic groups to act as nucleation sites for the formation of MOF.[27, 40] Herein we

find that SWCNTs nanotubes work better for the construction of FET sensors and are more amenable for dielectrophoresis (DEP).

A variety of nanotube to $Cu_3(HHTP)_2$ ratios were initially explored but final FET devices were fabricated using larger quantities of nanotubes (5% theoretical loading by mass) due to more favorable electronic behavior (Figure S1). Devices below 4% loading would commonly fail to generate devices due to low or zero conductivity. ox-SWCNTs failed to yield consistent devices until 10% loading was utilized (Figure S2). Physical morphology characterization of the formed composite materials was conducted utilizing electron microscopy (Figure 1). SWCNTs composites show relatively complete covering of nanotubes indicating the interaction is governed by π-π interactions (Figures 1a-c). In contrast, ox-SWCNTs based composites with same initial mass loading, show more clustered $Cu_3(HHTP)_2$ formation with numerous instances of bare nanotubes (Figures 1d-f). In both cases, no free $Cu_3(HHTP)_2$ was observed unassociated to nanotubes. Although DMF is a favorable solvent for suspending nanotubes, bundling of SWCNTs is still observed with minimal impact on resultant device performance. Additional TEM characterization of starting SWCNTs, ox-SWCNTs, SWCNTs@$Cu_3(HHTP)_2$, ox-SWCNTs@$Cu_3(HHTP)_2$ showed lengths and diameters consistent pre-/post-synthesis (Figure S3).

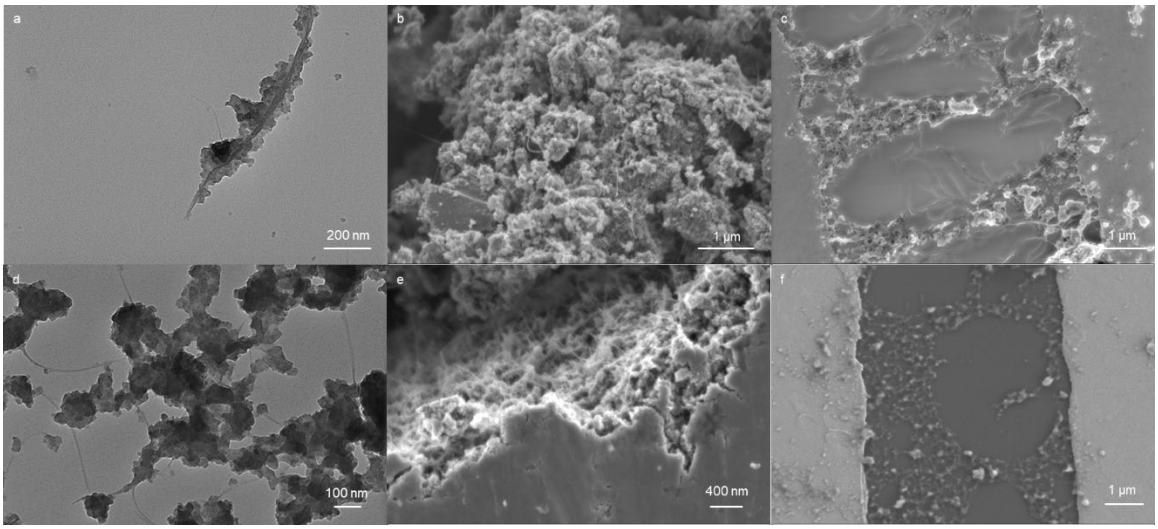

Figure 1: Electron microscopy of SWCNTs@$Cu_3(HHTP)_2$ composites. a) SWCNTs@$Cu_3(HHTP)_2$ with 5% mass loading of CNT on carbon backed TEM. b) SWCNTs@$Cu_3(HHTP)_2$ in powder form with clear nanotube dispersal throughout the structure. c) SWCNTs@$Cu_3(HHTP)_2$ deposited onto prefabricated devices with interdigitated gold electrodes. d,e,f) Similar micrographs as a,b,c but with ox-SWCNTs@$Cu_3(HHTP)_2$ instead of SWCNTs@$Cu_3(HHTP)_2$.

Observed SEM powders (Figures 1b and 1e) reveal homogeneous structure with intermixing of nanotubes and $Cu_3(HHTP)_2$. Tuning the mass loading alters the observed density of nanotubes (Figure S4). Nanorod morphology of $Cu_3(HHTP)_2$ is attenuated as compared to previous reports but this is attributed to large amounts of co-solvent. Nanorod morphology is more pronounced in lower nanotube concentrations due to reduction of co-solvent volume (Figure S5). $Cu_3(HHTP)_2$ synthesized without nanotubes still lack clear nanorod morphology (Figure S6). This indicates that absolute presence of co-solvent is more critical for perturbing the nanorod morphology formation rather than the relative amount.

Suspending powders in DMF by sonication with subsequent deposition onto interdigitated electrodes via dielectrophoresis (DEP)[62] yields structures (Figure 1c and 1f) that more closely resemble observed TEM than bulk powders. Sonication has been shown not to affect the overall microcrystalline structure even after 72 hours.[33] $Cu_3(HHTP)_2$ coverage on top of nanotubes is dense but not complete by simple observation. Retention of composite attachment through DEP processing and sonication indicates both π-π interactions and carboxylic groups have strong interactions to support composite materials through processing. DEP was chosen over previously used dropcasting to ensure thin layers of composite which are more amenable to liquid based FET measurements and are more easily subjected to liquid electrolyte gating.

Raman microscopy was utilized to understand the interface of $Cu_3(HHTP)_2$ on nanotubes both in terms of the relative presence or absence of peaks as well as shifting of known peaks (Figure 2a). Raman spectroscopy of carbon nanomaterials well-developed,[63] allowing for facile comparison of the $Cu_3(HHTP)_2$ growth. Analysis of $Cu_3(HHTP)_2$ powders with and without nanotubes reveal a complicated spectrum with the bulk of the features occurring between 1200 and 1600 cm^{-1} (Figure S7). The prominent features present in both nanotube composites are the radial breathing mode (RBM) at ~200 cm^{-1} and the 2D peak present at 2670 cm^{-1}. Minor redshifting of the RBM is observed in the composite, indicative of additional mass present on the nanotubes.[64] Typical analysis of relative D (1350 cm^{-1}):G (1600 cm^{-1}) ratios are precluded by the presence of $Cu_3(HHTP)_2$ vibration modes. Difficulty in achieving DEP deposition of ox-SWCNTs composite at similar mass loadings frustrates a comparative analysis of SWCNTs and ox-SWCNTs Raman peaks on silicon devices.

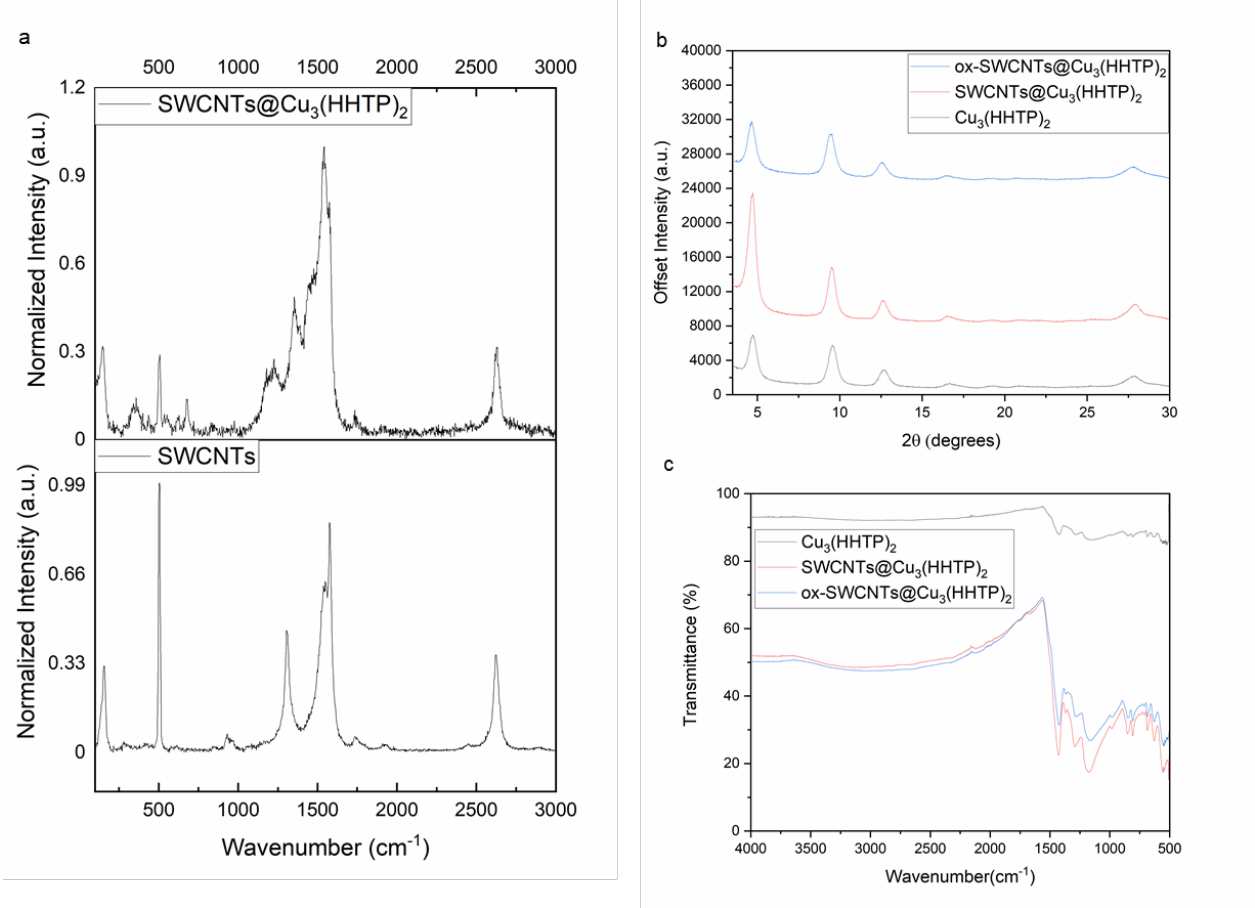

Figure 2: Raman spectroscopy, XRD, and FTIR spectroscopy of $Cu_3(HHTP)_2$, SWCNTs@$Cu_3(HHTP)_2$, and ox-SWCNTs@$Cu_3(HHTP)_2$. a) Raman spectra for bare SWCNTs and SWCNTs@$Cu_3(HHTP)_2$ deposited on prefabricated silicon devices. b) Stacked PXRD spectra for each of the different nanotube composite as well as $Cu_3(HHTP)_2$ without nanotubes. c) FTIR spectra for each of the different nanotube composite as well as $Cu_3(HHTP)_2$ without nanotubes.

Comparisons of microcrystalline structure through powder X-ray diffraction (PXRD) show minor variations depending on the presence of nanotubes (Figure 2b). In particular, the presence of SWCNTs shows larger relative growth of the 100 plane over other observed peaks. The 100 plane is primarily associated with the main pore presence in the structure and is suggestive of favorable growth of $Cu_3(HHTP)_2$ on π surfaces as compared to carboxylic groups. Both

$Cu_3(HHTP)_2$ as well as the ox-SWCNTs composite show expected peaks with minimal deviation from the known crystal pattern. The presence of carboxylic groups therefore does not impede the growth or substantially alter the microcrystalline structure.

FT-IR was used as a complementary technique to evaluate changes in MOF structure upon addition of nanotubes (Figure 2c). No differences in observed peaks were observed between the three cases of $Cu_3(HHTP)_2$, SWCNTs@$Cu_3(HHTP)_2$, and ox-SWCNTs@$Cu_3(HHTP)_2$. Observed spectra match previous reports[65] and indicated minimal effects of incorporation of nanotubes on the overall MOF structure.

UV-Vis absorption spectroscopy recapitulates the trend observed in XRD. As the proportion of nanotubes as well as co-solvent is increased, smaller and smaller amounts of $Cu_3(HHTP)_2$ growth can be observed as considered by a UV peak attributed to hexahydroxytriphenylene and a visible peak attributed to the coordinated Cu species (Figure S8).[66] As UV-Vis samples are prepared through post-synthetic suspension of known masses, the spectra represent insight into the relative proportion of $Cu_3(HHTP)_2$:SWCNT. Both $Cu_3(HHTP)_2$ as well as ox-SWCNTs@$Cu_3(HHTP)_2$ show relatively similar proportions as evaluated by peak height. This holds both as function of co-solvent volume as well as time. SWCNTs@$Cu_3(HHTP)_2$ shows comparatively higher growth as measured by peak height for the same measurements (Figure S9).

BET surface area measurements were also conducted for each of the different nanotube composite as well as $Cu_3(HHTP)_2$ without nanotubes (Figure S10). All the N_2 isotherms demonstrated type-I adsorption behavior with no hysteresis.[67] BET surface area was somewhat lower than previous reports (~520 m^2/g)[60] with $Cu_3(HHTP)_2$ having a surface area of (280 m^2/g). SWCNTs@$Cu_3(HHTP)_2$ had the largest surface area (420 m^2/g), and ox-SWCNTs@$Cu_3(HHTP)_2$ had a similar surface area to just the MOF alone (260 m^2/g). We attribute this reduced surface area

to relative short synthetic time (2 hours) as compared to previous synthesis (18 hours). The larger surface area of SWCNTs@$Cu_3(HHTP)_2$ composite is correlated with increased peak intensity observed in both UV-Vis as well as PXRD. This also indicate a potentially interesting structure directing effect or lower energy growth mechanism that could be leveraged for future applications. This is beyond the scope of the current work.

Composites of $Cu_3(HHTP)_2$ with carbon surfaces[60] have been made before but to the best of our knowledge this particular MOF has not been applied to single-walled carbon nanotubes (SWCNTs). SWCNTs are particularly attractive from a field-effect transistor (FET) sensing perspective due to the presence of semiconducting nanotubes. As-synthesized SWCNTs have a proportion of metallic nanotubes (1/3) which limits the usefulness in FET applications as metallic tubes are not easily modulated by an external charge environment. We note here in similarity to other efforts by our group,[27] that MOF growth on top of the nanotubes suppresses the metallic aspects of the present nanotubes. This gives strong evidence for either complete wrapping of nanotubes to prevent traditional electrical contact or at a minimum a percolation theory threshold[68] that is not exceeded. It has previously been noted that vary dilute networks of unsorted SWCNTs can have more semiconducting nature even with the presence of metallic nanotubes. This can be rationalized as a decreasing quantity of metallic nanotube junctions which increase the overall resistance of the nanotube network. By including an additional material, $Cu_3(HHTP)_2$, again the quantity of these nanotube junctions is lowered, and a more semiconducting network is established. Additional considerations for making devices here include a preference for DEP as compared to drop casting to achieve much thinner films which are more reliably gated in liquid electrolyte. Device fabrication was also considerably improved by utilizing DMF as the solvent for the suspension instead of H_2O. We hypothesize that this is due to relative lowering of the dielectric

constant which means less effect screening of the AC field and consequently more force to pull the composites to the surface. At higher relative concentrations of $Cu_3(HHTP)_2$ to nanotube, devices cannot achieve sufficient electrical contact between SWCNTs to make viable FET devices. This indicates a percolation mechanism governing the overall electric properties of the composite material. At the two highest concentrations (5 and 10% respectively) explored (Figure S11), good devices with tens to hundreds of microamps in on-current can be manufactured utilizing unoxidized nanotubes. Oxidized nanotubes generate consistent devices only at 10% mass loading (Figure S2).

This difference in the electrical properties of the devices points to key differences in how nanotube functionalization affects the orientation and overall properties of the resulting devices. We chose to focus on unoxidized nanotubes for electrical device testing to have multiple loadings to compare initial sensing results against. Without salts present in the gating solution, devices show relatively poor gate modulation of the current. Introduction of 100 mM KCl dramatically improves the gating performance with on/off current ratios typically exceeds 20. Current on/off ratios for SWCNTs are typically beneath one unless devices are sparsely generated. Off-current is dictated by the CNT junction resistance and the presence of metallic nanotubes.

We explored the sensing of a homologous series of glucose monomers including glucose, maltose, maltotriose, α-, β-, and γ- cyclodextrin (CD) as a test case for size selective sensing (Figure 3). FET sensing is typically modulated by the presence of small molecules which affect the overall chemical potential of the device.[69] Distinguishing analytes is typically conducted by choosing materials which have radically different chemical character (either electron donating, electron withdrawing, polar, or preferential interaction with the surface). Here we demonstrate molecular differentiation solely based on size of analyte instead of chemical functionalities

present. The proposed mechanism for this sensing is the obstruction of pores by smaller units of the series which inhibit the transport of ions to the surface of the nanotubes altering the gate capacitance of the composite.[70]

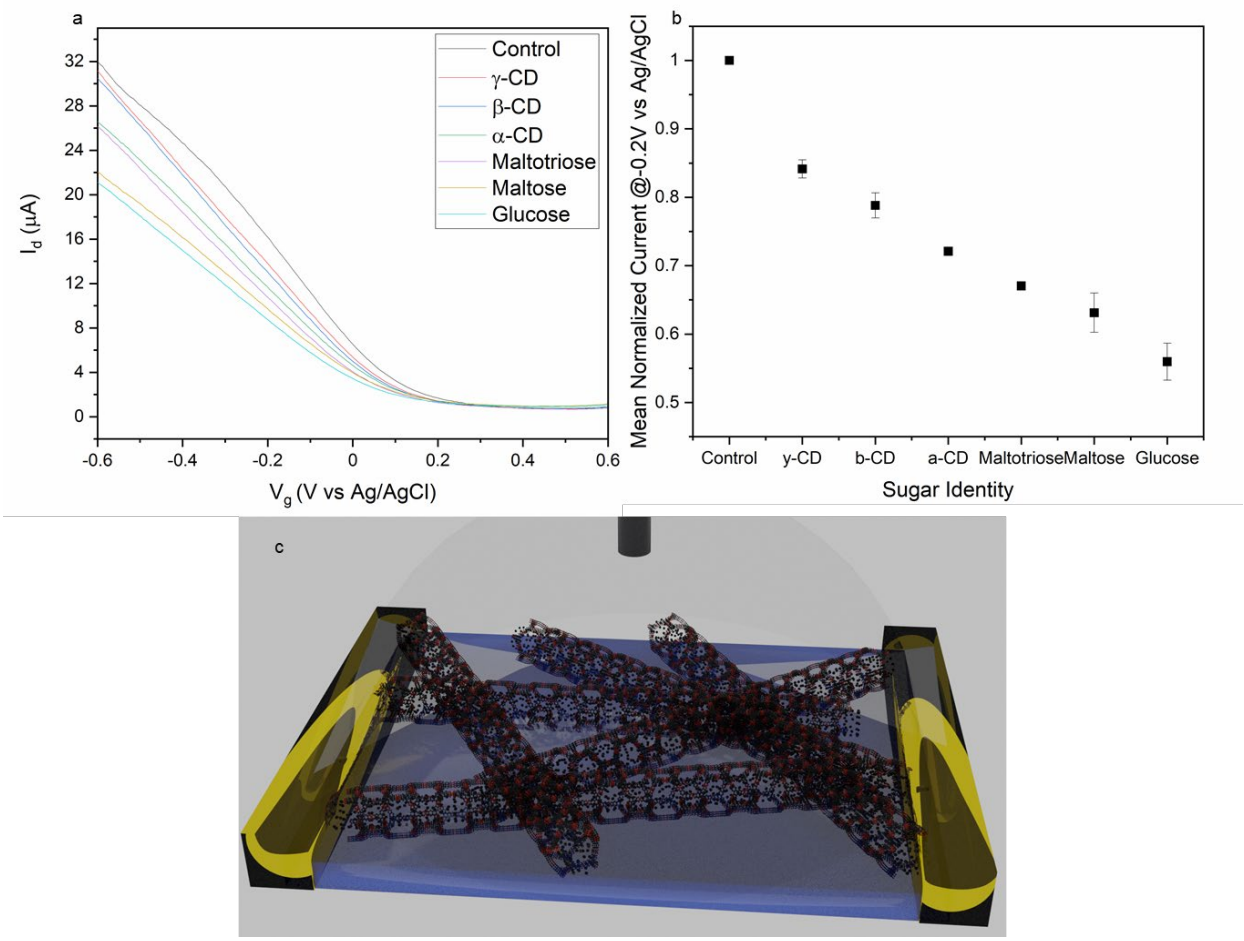

Figure 3: Liquid gated FET demonstrating size selective changes in current. a) FET curves with different size carbohydrates measured serially in constant ionic strength. b) Mean ± SD current for (n = 3) devices displayed in panel a. Devices are normalized to current with no sugar molecules present @ –0.2 V vs Ag/AgCl. c) Illustration of liquid FET sensing using SWCNTs@$Cu_3(HHTP)_2$.

Measuring different saccharide units at equivalent concentrations (500 μM) in the same ionic strength KCl solution reveals a decreasing current on the p-branch of the nanotubes as the size of the sugar is decreased (Figure 3a). Larger sugars, which should not necessarily enter the pores, also affect the capacitance indicating that gaps in $Cu_3(HHTP)_2$ coverage on the SWCNTs. Sugars interacting with bare SWCNTs also block the transit of ions to the surface. This trend holds across different synthetic runs and even after several months in solution before deposition onto devices. Bending of the curve in this manner is equivalent to a reduction in gate capacitance. Additional titration measurements reveal a concentration dependent reduction of current in the p-branch of the FET curve for glucose (Figure S12). Limits of detection are in the single digit micromolar range made by evaluating the conductance at –0.4 V vs Ag/AgCl (Figure S13). Making evaluations at the most negative gate voltage results can lead to spurious results due to effect of changing ionic strength in a titration experiment. The observed decrease in p-branch current is on a time scale similar to the length of the measurement as no change is observed at the highest concentrations for repeated measurements after five and ten minutes (Figure S14).

Further confirmation of size selective sensing can be ascertained from running titrations without washing off devices in between measurements. Initial introduction of glucose followed by other sugars in ascending sequence of size yields the largest current decrease with glucose (Figure S15). The addition of other sugar solutions decreases the overall concentration of glucose in the solution increasing the observed current but is still differentiable from the measurements made in the absence of sugar molecules in each case. Titration experiments running from the largest sugar unit, γ-CD, to the smallest, glucose, reveal similar trends in current (Figure S16). The lowest current for the p-branch is always with the glucose testing revealing a size selective behavior for

the response in the FET curve. Consistence in the observed minimal current is strong evidence for the filling of the pores of $Cu_3(HHTP)_2$ as a dominant mechanism in modulating gate capacitance.

No trend in gate modulation is observed with only SWCNTs deposited on a device indicating the crucial presence of the MOF (Figure S17). If the relative concentration of the nanotubes is increased to 10%, the observed effect is decreased, indicating that the thickness of the $Cu_3(HHTP)_2$ also crucially modulates the effect (Figure S18). Higher ratios of $Cu_3(HHTP)_2$ to SWCNTs induce less favorable electronic characteristics. We therefore have optimized around an intermediate loading of 5% to achieve maximal sensing response without sacrificing conductivity. Minimal change is observed upon simple dilution of the solution indicating the presence of the sugar units as crucial to achieve observed gate modulation (Figure S19).

Sweeping gate voltage in the opposite direction yields similar differentiation between the presence and absence of glucose. Repeated scans in the reverse direction also show minimal differences in current indicating that the initial pore filling process is rapid and observed behavior is not a transient effect (Figure S20). Additional FET measurements with a slower gate voltage sweep show decreased current indicating that the capacitance is indeed reduced and the observed reduced capacitance is minimally affected by the rate at which the gate voltage is swept (Figure S21).

In the interest of understanding the effect of ionic strength on the measurements, we performed additional experiments with and without glucose presence in solutions with increasing ionic strength (Figure 4). As ionic strength is increased, both threshold voltage shifts to more negative potentials as well as higher current at the most negative gate voltages are observed. To demonstrate the relative effect of glucose in different ionic strength environments we plot the current observed at –200 mV vs Ag/AgCl reference for a range of ionic strengths from 1 mM to 1

M in order of magnitude steps. The observed effect in the presence of glucose is a decreasing change in slope indicative of lower ionic strength due to pore blocking.

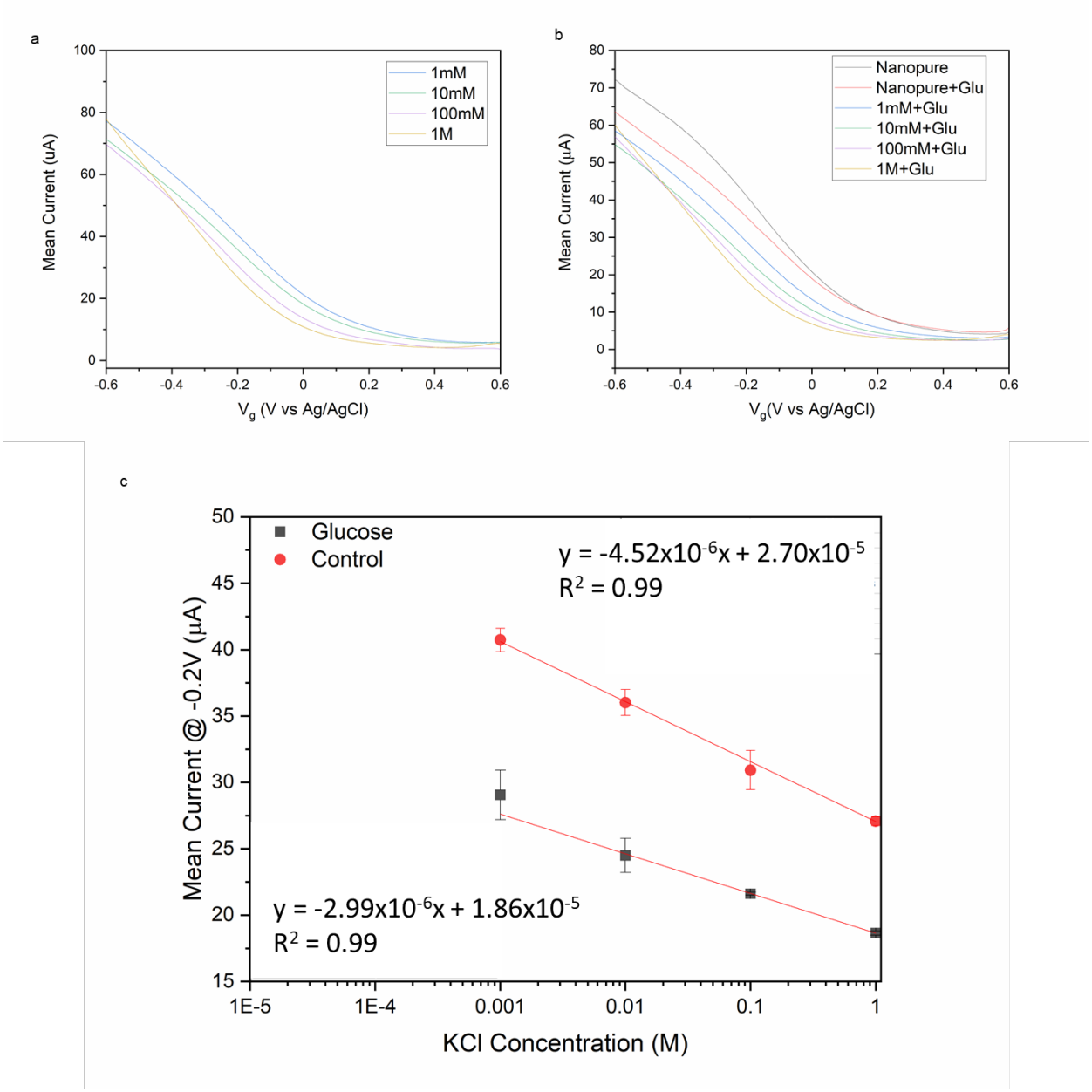

Figure 4: FET curves of SWCNTs@$Cu_3(HHTP)_2$ composite at 5% loading by mass in increasing ionic strength environments. Each measurement was made in triplicate to yield mean curves

displayed here. a) Without glucose, b) with glucose, c) comparison of current at –200 mV vs Ag/AgCl in increasing ionic strength environments.

To better understand the relationship between measured current and sugar identity, we performed a series of molecular dynamics (MD) simulations using LAMMPS.[46] Specifically, we modeled the diffusion of K^+ ions through $Cu_3(HHTP)_2$ with varying concentrations and species of sugars in the pores. The rationale was to examine if differences in observed current were related to the varying diffusivities of ions through the pores as a function of sugar identity.

Although the sensing effect is observed in the composite material only, we focused our calculations on just the $Cu_3(HHTP)_2$ for the following reasons. All of the material's characterization point to MOF being the overwhelming majority component in the composite. The electron microscopy indicates that layers of MOF are present in minimal thickness of 100 nm around a given SWCNT structure. Rough calculation reveals 300 layers of MOF, the vast majority of which experience minimal structural change from the being co-located with the SWCNTs. Additionally, placing SWCNTs into the periodic boundary calculations would be computationally prohibitive due to necessary unit cell size. Finally, as the determined sensing effect is dependent on the MOF pore clogging we expect these computations to capture the majority of the effect.

Although many factors can potentially affect the diffusion of ions through the pores of a MOF, we chose to initially focus on a simple model that considered primarily geometric effects and simplified energetic interactions. In particular, we applied the following simplifications: (1) the solvation environment (i.e., dissolved ions + water) was ignored, which is equivalent to an implicit solvation model in the high dielectric screening limit (where interactions from charged species are screened over very short distances), (2) in this limit, Coulombic interactions were ignored and the ion was modelled as a Lennard-Jones (LJ) sphere where solvation-shell effects

could be approximated by controlling the radius of the sphere, and (3) lastly, we assumed that the vibrations of the atoms of the MOF crystal would not significantly affect ion diffusion relative to other factors, and so we held them rigid throughout the simulations.

Structure files were prepared by inserting the sugars, and the LJ sphere representing the ion, into the pore of the MOF into trial positions/configurations. Due to the lack of availability of either crystallographic data, or a DFT-optimized structure, for $Cu_3(HHTP)_2$, we instead used $Ni_3(HHTP)_2$, which was obtained from Xu et al.[47] and is expected to have a nearly identical structure. The positions of the sugars within the MOF were then optimized in Avogadro[48] using Universal Force Field (UFF) parameters,[49] with the positions of the framework atoms and ion fixed. This step ensured that the bonding was correctly determined when generating LAMMPS input files. The LAMMPS input files were prepared using the "lammps-interface" repository by Boyd et al.,[50] which was used to assign UFF parameters to all atoms in the system. Additionally, the unit cells were replicated once in each direction during this step, resulting in a 2x2x2 supercell, for a total of 8 ions represented by LJ spheres in the system.

Since the density of adsorbed sugars in the MOF was unknown, we ran multiple simulations, varying the number of sugar molecules per pore from one up to a maximum determined by crossing 32.5% of the pore volume according to a simple geometric calculation (see Supporting Information).

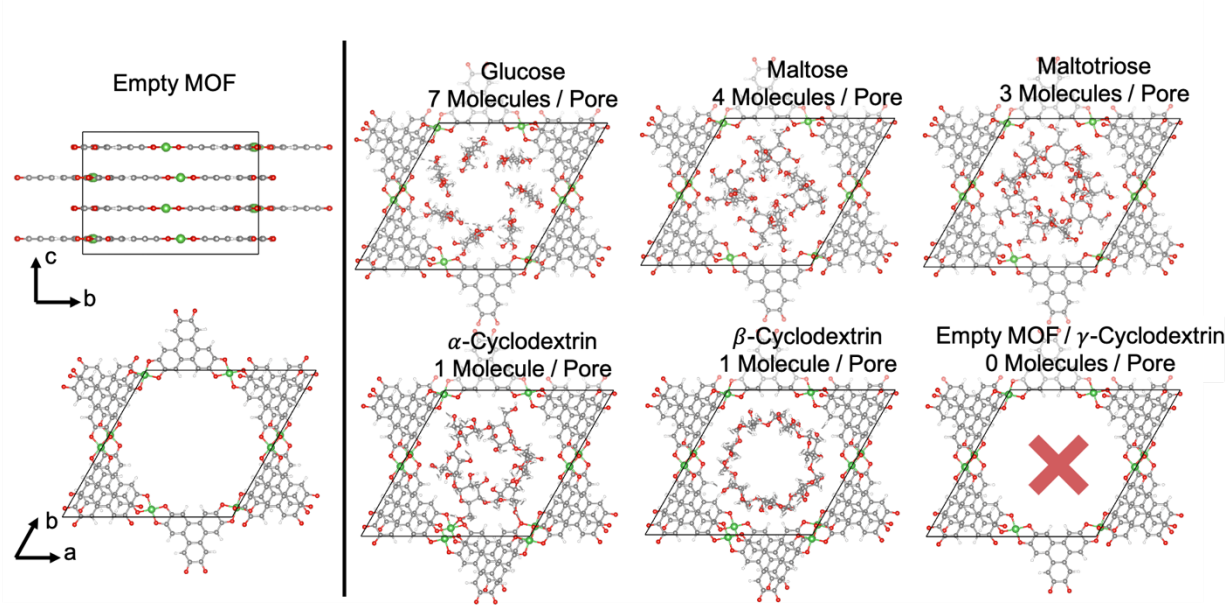

Figure 5. 1x1x1 unit cells for both an empty MOF and each of the maximally packed configurations. Atoms extending beyond the cell border are part of the neighboring unit cells but are shown for clarity. Note that γ-CD does not fit inside the pore, and thus is modelled by an empty MOF.

Molecular dynamics simulations were run in LAMMPS using the NVT ensemble for 5 million 0.5 fs timesteps, for a total simulation length of 250 ps. The temperature was set to 450 K to accelerate diffusion rates for better sampling efficiency (below 0.1 $Å^2$/ps, simulations become prohibitively expensive to run without specialized sampling techniques). The mean-squared displacement of each of the 8 ions (represented by LJ spheres) was individually tracked, along with average mean-squared displacement, from which the diffusion coefficient was extracted (see **Figure 6**).

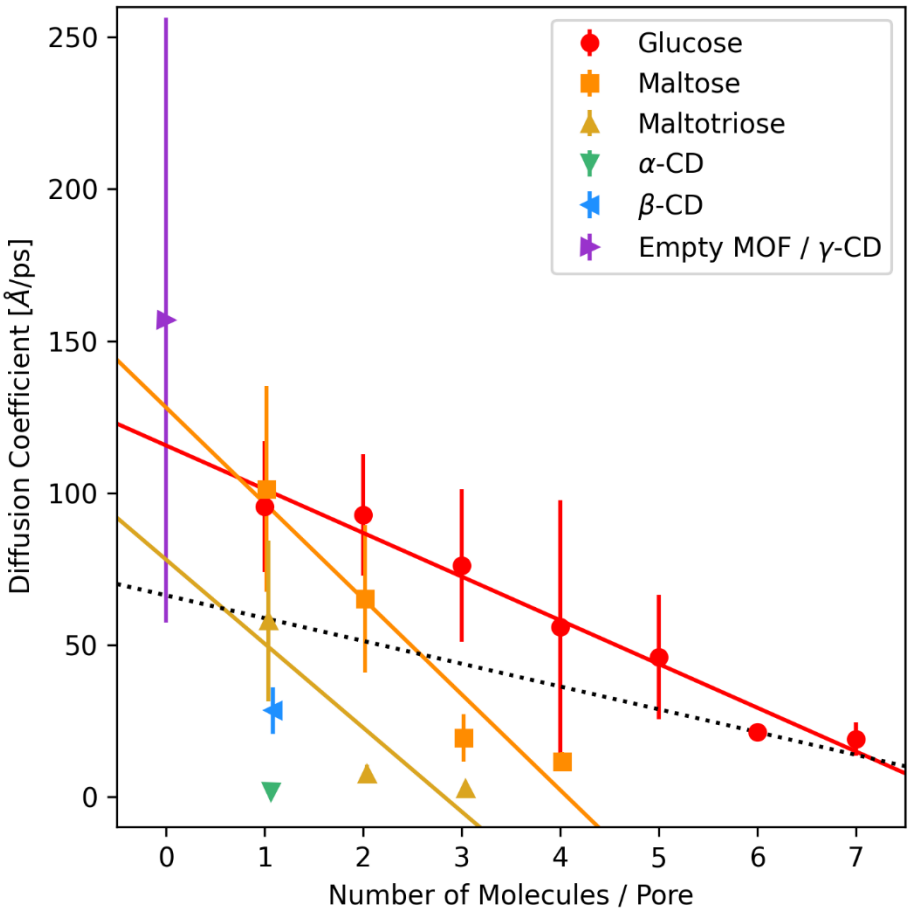

Figure 6. Plot of the calculated diffusion coefficients as a function of the number of sugar(s) in the pore of the MOF. The solid lines show the line of best fit for each of the sugars, and the dashed black line represents the approximate sugar packing trend.

As expected, ion diffusivity decreases as sugars are more densely packed into the pores, and, with only one exception, large sugar molecules impede diffusion more than small molecules. The exception we observed was for β-CD, where ion diffusivity was substantially higher than for α-CD, the smaller of the two sugar molecules. This is likely due to the large open space in the center of beta-cyclodextrin which makes for an ideal diffusion pathway, whereas it is difficult for an ion to diffuse either through the center of α-CD or between the wall of the MOF and the sugar.

This result is consistent with the experimental observations of decreased current with increased glucose concentration (see Figure S13 in the Supporting Information). From these observations, we speculate that for the smaller sugar molecules the pores are likely more tightly packed (i.e., 6-7 molecules per pore for glucose and 3-4 molecules per pore for maltose), and only loosely packed pores for large molecules (i.e., 1 molecule per pore for maltotriose). Under such a packing arrangement, one might expect ion diffusivity through the MOF pores to generally increase as function of the size of the adsorbed sugars, as evidenced by the dashed line in Figure 5. Additional experimental evidence for sugars decreasing ion diffusivity comes from cyclic voltammetry with an inorganic redox probe. Changes in the slope of the peak current versus the square root of the scan rate show reduced diffusivity in the presence of glucose as compared to α-CD (Figure S22).

One similar rationale for this behavior could be the presence of a concentration gradient of the sugars within the pores. As the sugars increase in size, they will diffuse more slowly through the pore, partially because of their size relative to the pore, and partially because their diffusion will be further impeded by other large sugar molecules. Conversely, small sugar molecules will diffuse more freely, and thus pack the pores quicker and more uniformly. This notion is corroborated by the FET titration experiments (see Figures S15 and S16 in the Supporting Information), in which the largest change in current results from the introduction of glucose, regardless of whether the glucose is introduced before or after the larger sugar molecules. This suggests that the diffusion of ions through the pores packed with large sugar molecules should be represented by a blend of empty pores and sugar-packed pores, whereas for small sugar molecules, the diffusion of the ions is better represented by the uniform packing of sugars. Because the simulations are periodic, it becomes much harder to simulate the first scenario without using prohibitively large simulation

boxes. The second scenario, however, is much easier to simulate since the implicit assumption of periodic boundary conditions is that the concentration of sugars is uniform. Consequently, the difference between the observed and simulated trends, specifically for the α- and β-cyclodextrin can be explained as an overpacking of the pores in the simulations. Further exploration of the packing of the pores and refinement of the initial assumptions could provide additional insights into the behavior of the sensors, but these results suggest that size-selective sensing can be achieved on the basis of ion diffusivity.

Conclusions

Here we present a methodology for size selective sensing of sugars utilizing SWCNTs@$Cu_3(HHTP)_2$ hybrids. We have demonstrated changes in resulting morphology, microcrystalline structure, and surface area conditional upon the presence of carboxylic groups on the surface of nanotubes as well as absolute quantity of co-solvent present in the synthesis. Only larger relative loadings of CNTs (>5% by mass) yield well-behaved electrical devices which can be deposited on interdigitated electrodes via DEP. Lack of carboxylic groups enables deposition at lower mass loadings for the resulting composites. As-deposited composite materials show enhanced semiconducting characteristics as compared to unfunctionalized nanotubes evidenced by improved current on/off ratios.

FET devices show size dependent changes in current dependent on the size of the sugar unit for a homologous series of sugars ranging from eight glucose units to one unit. Glucose shows the largest decrease in current due to pore filling which alters the gate capacitance. Current is modified for in the presence of glucose in a linear fashion dependent on the concentration. Titration of FET devices from either largest to smallest or vice versa yields the lowest current for glucose. Measuring in a series of increasing ionic strengths, the presence of glucose shows smaller changes

in current at –200 mV indicating the effect of glucose as alteration of the capacitive strength of the environment. MD simulations indicate that mobile ions in the gating solution will experience decreased diffusivity based on the size of carbohydrate molecule present supporting the experimentally observed decreased gate capacitance.

We believe the sensing methodology presents a new way to evaluate molecules in complex environments and provides a way to reliably discriminate on the basis of size. MOF composites with SWCNT remain a nascent field and the potential structural diversity of MOFs would enable large ranges of sizes to be explored. This work represents several important advances in demonstrating size selective FET sensing, development of synthetic methodology to combine MOFs with SWCNT, and improved SWCNT@MOF composite device manufacture.

Experimental:

Suspension of Carbon Nanotubes

For composites, either unoxidized single-walled carbon nanotubes (SWCNT, P2 Carbon Solutions) or oxidized single-walled carbon nanotubes (ox-SWCNT, P3 Carbon Solutions) were prepared into 0.1 mg/mL solutions of DMF. DMF solutions were sonicated for one hour to suspend nanotubes yielding a dark black solution. Suspended nanotubes were centrifuged for 30 mins at 3000 rpm to remove large aggregates and bundles. 90% of the supernatant was recovered and used for the $Cu_3(HHTP)_2$ synthesis. A small aliquot of both the SWCNTs and ox-SWCNTs nanotubes were taken to measure UV-Vis characteristics. Concentrations of nanotubes used for the synthesis were normalized according to the observed intensity at 550 nm.

$Cu_3(HHTP)_2$ growth with and without nanotubes

$Cu_3(HHTP)_2$ was synthesized from a previously published adapted procedure.[60] For small scale syntheses to investigate the effects of mass loading of nanotubes, the following conditions were used. $Cu_3(HHTP)_2$ precursors, 8 mg of copper (II) acetate monohydrate and 6.5 mg of 2,3,6,7,10,11-hexahydroxytriphenylene (HHTP), were massed and placed into either a 1-dram vial or 20 mL scintillation vial. Mass loading of nanotubes was controlled by changing the volume of the reaction. For instance, in the case of 0.5% loading, 0.5mL of the previously generated suspended nanotube DMF solution was added to 0.5mL of deionized water along with the copper and HHTP precursors. This mixture was sonicated for 20 minutes and then placed into an oven at 85 ºC for two hours. The reaction mixture was removed and allowed to cool to room temperature. The resulting mixture was washed three times with both H_2O and acetone and the final product was left to dry in a vacuum oven at 65 ºC for 18 hours under reduced pressure to yield a black powder. Large scale syntheses for the 5% mass loading were also conducted in very similar conditions with the primary difference of using 80 mg of the copper precursor, 65 mg of HHTP, 50 mL of the SWCNT/DMF solution and 50 mL of water. $Cu_3(HHTP)_2$ without nanotubes present were synthesized by using laboratory DMF.

DEP Deposition on prefabricated silicon devices

SWCNTs@$Cu_3(HHTP)_2$ powders at various mass loadings were sonicated into DMF at a concentration of 0.1 mg/mL for a total of one hour. Suspended solutions took on a deep blue color. These solutions were used for dielectrophoresis on prefabricate silicon devices with interdigitated electrodes with the following conditions: 60 µL of SWCNTs@$Cu_3(HHTP)_2$ in DMF solution, 100 kHz frequency, 10 V of peak to peak voltage for two minutes. Devices were immediately washed with water and blown dry with N_2. Devices were left on a hotplate at 120 ºC for 30 minutes before any FET measurements to remove residual solvent.

FET Sensing of sugars

Glucose, maltose, maltotriose, α-, β-, and γ- cyclodextrin (CD) samples were prepared in 1 mM concentrations utilizing deionized water as the solvent. Measurements for constant ionic strength were conducted by initially placing 100 mM KCl with deionized water in a 1:1 proportion on devices. The solution was in contact with an Ag/AgCl reference electrode. A 50 mV source drain bias was applied while gate voltages were swept from +600 mV to –600 mV in 200 total steps taking a total of 24 seconds. After this initial test, devices were washed with deionized water and blown dry with N_2 before the next test was conducted. This cycle was repeated for each sugar solution replacing the deionized water with the appropriate 1 mM sugar solution.

For titration measurements, an initial set of measurements with the 1:1 100 mM KCl:deionized water was conducted. An addition equal volume aliquot of deionized water was then introduced without washing off the device. Electrical measurements followed the same parameters as above. This experiment was repeated as many times as the titration required. Comparatively little changes caused by dilution of the electrolyte were observed as compared to presence of sugars.

ASSOCIATED CONTENT

Supporting Information. Additional details on experimental methods, electron microscopy, FET curves, UV-Vis spectra, Raman Spectra, Cyclic Voltammograms, and Nitrogen adsorption isotherms. This material is available free of charge via the Internet at http://pubs.acs.org.

Corresponding Author

* Alexander Star

Email: astar@pitt.edu

Author Contributions

The manuscript was written through contributions of all authors. All authors have given approval to the final version of the manuscript.

ACKNOWLEDGMENT

The work was supported by the National Science Foundation under Grant No. 2003302. The XplorA Raman-AFM/TERS system was purchased via Defense University Research Instrumentation Program (DURIP) grant from the Office of Naval Research, ONR (N000141410765).

We gratefully acknowledge support from the University of Pittsburgh's Swanson School of Engineering and the Center for Research Computing for computational resources.

References

1. Ellis, J. E.; Star, A., Carbon Nanotube Based Gas Sensors toward Breath Analysis. *ChemPlusChem* **2016,** *81*, 1248-1265.
2. Weis, J. G.; Ravnsbæk, J. B.; Mirica, K. A.; Swager, T. M., Employing halogen bonding interactions in chemiresistive gas sensors. *ACS Sens.* **2016,** *1*, 115-119.
3. Park, C. H.; Schroeder, V.; Kim, B. J.; Swager, T. M., Ionic Liquid-Carbon Nanotube Sensor Arrays for Human Breath Related Volatile Organic Compounds. *ACS Sens.* **2018,** *3*, 2432-2437.
4. Lapointe, F.; Ding, J.; Lefebvre, J., Carbon Nanotube Transistors as Gas Sensors: Response Differentiation Using Polymer Gate Dielectrics. *ACS Appl. Polym. Mater.* **2019**, *12,* 3269-3278.
5. Hwang, S. I.; Franconi, N. G.; Rothfuss, M. A.; Bocan, K. N.; Bian, L.; White, D. L.; Burkert, S. C.; Euler, R. W.; Sopher, B. J.; Vinay, M. L., Tetrahydrocannabinol detection using semiconductor-enriched single-walled carbon nanotube chemiresistors. *ACS Sens.* **2019,** *4*, 2084-2093.
6. Chen, Y.; Mun, S. C.; Kim, J., A wide range conductometric pH sensor made with titanium dioxide/multiwall carbon nanotube/cellulose hybrid nanocomposite. *IEEE Sens. J.* **2013,** *13*, 4157-4162.
7. Li, C. A.; Han, K. N.; Pham, X. H.; Seong, G. H., A single-walled carbon nanotube thin film-based pH-sensing microfluidic chip. *Analyst* **2014,** *139*, 2011-5.
8. Gou, P.; Kraut, N. D.; Feigel, I. M.; Bai, H.; Morgan, G. J.; Chen, Y.; Tang, Y.; Bocan, K.; Stachel, J.; Berger, L.; Mickle, M.; Sejdic, E.; Star, A., Carbon nanotube chemiresistor for wireless pH sensing. *Sci. Rep.* **2014,** *4*, 4468.
9. Kaempgen, M.; Roth, S., Transparent and flexible carbon nanotube/polyaniline pH sensors. *J. Electroanal. Chem.* **2006,** *586*, 72-76.
10. Morton, J.; Havens, N.; Mugweru, A.; Wanekaya, A. K., Detection of trace heavy metal ions using carbon nanotube-modified electrodes. *Electroanalysis* **2009,** *21*, 1597-1603.

11. Tung, N. T.; Tue, P. T.; Thi Ngoc Lien, T.; Ohno, Y.; Maehashi, K.; Matsumoto, K.; Nishigaki, K.; Biyani, M.; Takamura, Y., Peptide aptamer-modified single-walled carbon nanotube-based transistors for high-performance biosensors. *Sci. Rep.* **2017,** *7*, 17881.
12. Sun, Y.; Peng, Z.; Li, H.; Wang, Z.; Mu, Y.; Zhang, G.; Chen, S.; Liu, S.; Wang, G.; Liu, C.; Sun, L.; Man, B.; Yang, C., Suspended CNT-Based FET sensor for ultrasensitive and label-free detection of DNA hybridization. *Biosens. Bioelectron.* **2019,** *137*, 255-262.
13. Viswanathan, S.; Wu, L.-c.; Huang, M.-R.; Ho, J.-a. A., Electrochemical immunosensor for cholera toxin using liposomes and poly (3, 4-ethylenedioxythiophene)-coated carbon nanotubes. *Anal. Chem.* **2006,** *78*, 1115-1121.
14. Sharf, T.; Wang, N. P.; Kevek, J. W.; Brown, M. A.; Wilson, H.; Heinze, S.; Minot, E. D., Single electron charge sensitivity of liquid-gated carbon nanotube transistors. *Nano Lett.* **2014,** *14*, 4925-30.
15. Kong, J.; Franklin, N. R.; Zhou, C.; Chapline, M. G.; Peng, S.; Cho, K.; Dai, H., Nanotube molecular wires as chemical sensors. *Science* **2000,** *287*, 622-625.
16. Puchades, I.; Lawlor, C. C.; Schauerman, C. M.; Bucossi, A. R.; Rossi, J. E.; Cox, N. D.; Landi, B. J., Mechanism of chemical doping in electronic-type-separated single wall carbon nanotubes towards high electrical conductivity. *J. Mat. Chem. C* **2015,** *3*, 10256-10266.
17. Kaskela, A.; Nasibulin, A. G.; Timmermans, M. Y.; Aitchison, B.; Papadimitratos, A.; Tian, Y.; Zhu, Z.; Jiang, H.; Brown, D. P.; Zakhidov, A.; Kauppinen, E. I., Aerosol-synthesized SWCNT networks with tunable conductivity and transparency by a dry transfer technique. *Nano Lett.* **2010,** *10*, 4349-55.
18. Yoon, I.; Eom, G.; Lee, S.; Kim, B. K.; Kim, S. K.; Lee, H. J., A Capacitive Micromachined Ultrasonic Transducer-Based Resonant Sensor Array for Portable Volatile Organic Compound Detection with Wireless Systems. *Sensors (Basel)* **2019,** *19*, 1401.
19. Odom, T. W.; Huang, J.-L.; Kim, P.; Lieber, C. M., Atomic structure and electronic properties of single-walled carbon nanotubes. *Nature* **1998,** *391*, 62-64.
20. Ouyang, M.; Huang, J. L.; Lieber, C. M., Fundamental electronic properties and applications of single-walled carbon nanotubes. *Acc. Chem. Res.* **2002,** *35*, 1018-25.
21. Bekyarova, E.; Itkis, M. E.; Cabrera, N.; Zhao, B.; Yu, A.; Gao, J.; Haddon, R. C., Electronic properties of single-walled carbon nanotube networks. *J. Am. Chem. Soc.* **2005,** *127*, 5990-5.
22. Tasis, D.; Tagmatarchis, N.; Bianco, A.; Prato, M., Chemistry of carbon nanotubes. *Chem. Rev.* **2006,** *106*, 1105-1136.
23. Wang, F.; Swager, T. M., Diverse chemiresistors based upon covalently modified multiwalled carbon nanotubes. *J. Am. Chem. Soc.* **2011,** *133*, 11181-11193.
24. Huang, J.; Ng, A. L.; Piao, Y.; Chen, C. F.; Green, A. A.; Sun, C. F.; Hersam, M. C.; Lee, C. S.; Wang, Y., Covalently functionalized double-walled carbon nanotubes combine high sensitivity and selectivity in the electrical detection of small molecules. *J. Am. Chem. Soc.* **2013,** *135*, 2306-12.
25. Steuerman, D. W.; Star, A.; Narizzano, R.; Choi, H.; Ries, R. S.; Nicolini, C.; Stoddart, J. F.; Heath, J. R., Interactions between conjugated polymers and single-walled carbon nanotubes. *J. Phys. Chem. B* **2002,** *106*, 3124-3130.
26. Tang, B. Z.; Xu, H., Preparation, alignment, and optical properties of soluble poly (phenylacetylene)-wrapped carbon nanotubes. *Macromolecules* **1999,** *32*, 2569-2576.
27. Ellis, J. E.; Zeng, Z.; Hwang, S. I.; Li, S.; Luo, T. Y.; Burkert, S. C.; White, D. L.; Rosi, N. L.; Gassensmith, J. J.; Star, A., Growth of ZIF-8 on molecularly ordered 2-

methylimidazole/single-walled carbon nanotubes to form highly porous, electrically conductive composites. *Chem. Sci.* **2019,** *10*, 737-742.
28. Stavila, V.; Talin, A. A.; Allendorf, M. D., MOF-based electronic and opto-electronic devices. *Chem. Soc. Rev.* **2014,** *43*, 5994-6010.
29. Day, R. W.; Bediako, D. K.; Rezaee, M.; Parent, L. R.; Skorupskii, G.; Arguilla, M. Q.; Hendon, C. H.; Stassen, I.; Gianneschi, N. C.; Kim, P.; Dinca, M., Single Crystals of Electrically Conductive Two-Dimensional Metal-Organic Frameworks: Structural and Electrical Transport Properties. *ACS Cent. Sci.* **2019,** *5*, 1959-1964.
30. Hmadeh, M.; Lu, Z.; Liu, Z.; Gándara, F.; Furukawa, H.; Wan, S.; Augustyn, V.; Chang, R.; Liao, L.; Zhou, F.; Perre, E.; Ozolins, V.; Suenaga, K.; Duan, X.; Dunn, B.; Yamamto, Y.; Terasaki, O.; Yaghi, O. M., New Porous Crystals of Extended Metal-Catecholates. *Chem. Mater.* **2012,** *24*, 3511-3513.
31. Xie, L. S.; Skorupskii, G.; Dinca, M., Electrically Conductive Metal-Organic Frameworks. *Chem. Rev.* **2020,** *120*, 8536-8580.
32. Hinckley, A. C.; Park, J.; Gomes, J.; Carlson, E.; Bao, Z., Air-Stability and Carrier Type in Conductive M3(Hexaaminobenzene)2, (M = Co, Ni, Cu). *J. Am. Chem. Soc.* **2020,** *142*, 11123-11130.
33. Ko, M.; Mendecki, L.; Eagleton, A. M.; Durbin, C. G.; Stolz, R. M.; Meng, Z.; Mirica, K. A., Employing Conductive Metal-Organic Frameworks for Voltammetric Detection of Neurochemicals. *J. Am. Chem. Soc.* **2020,** *142*, 11717-11733.
34. Mahringer, A.; Jakowetz, A. C.; Rotter, J. M.; Bohn, B. J.; Stolarczyk, J. K.; Feldmann, J.; Bein, T.; Medina, D. D., Oriented Thin Films of Electroactive Triphenylene Catecholate-Based Two-Dimensional Metal-Organic Frameworks. *ACS Nano* **2019,** *13*, 6711-6719.
35. Okur, S.; Qin, P.; Chandresh, A.; Li, C.; Zhang, Z.; Lemmer, U.; Heinke, L., An enantioselective e-nose: An array of nanoporous homochiral MOF films for stereospecific sensing of chiral odors. *Angewandte Chemie International Edition* **2021,** *60*, 3566-3571.
36. Yao, M. S.; Lv, X. J.; Fu, Z. H.; Li, W. H.; Deng, W. H.; Wu, G. D.; Xu, G., Layer-by-Layer Assembled Conductive Metal–Organic Framework Nanofilms for Room-Temperature Chemiresistive Sensing. *Angewandte Chemie* **2017,** *129*, 16737-16741.
37. Yao, M. S.; Xiu, J. W.; Huang, Q. Q.; Li, W. H.; Wu, W. W.; Wu, A. Q.; Cao, L. A.; Deng, W. H.; Wang, G. E.; Xu, G., Van der Waals Heterostructured MOF-on-MOF Thin Films: Cascading Functionality to Realize Advanced Chemiresistive Sensing. *Angewandte Chemie* **2019,** *131*, 15057-15061.
38. Campbell, M. G.; Liu, S. F.; Swager, T. M.; Dincă, M., Chemiresistive sensor arrays from conductive 2D metal–organic frameworks. *Journal of the American Chemical Society* **2015,** *137*, 13780-13783.
39. Allendorf, M. D.; Dong, R.; Feng, X.; Kaskel, S.; Matoga, D.; Stavila, V., Electronic devices using open framework materials. *Chemical Reviews* **2020,** *120*, 8581-8640.
40. Zeng, Z.; Sorescu, D. C.; White, D. L.; Hwang, S. I.; Shao, W.; He, X.; Schulte, Z. M.; Rosi, N. L.; Star, A., Heterogeneous Growth of UiO-66-NH2 on Oxidized Single-Walled Carbon Nanotubes to Form "Beads-on-a-String" Composites. *ACS Applied Materials & Interfaces* **2021**.
41. Cortés-Súarez, J.; Celis-Arias, V.; Beltrán, H. I.; Tejeda-Cruz, A.; Ibarra, I. A.; Romero-Ibarra, J. E.; Sánchez-González, E.; Loera-Serna, S., Synthesis and characterization of an SWCNT@ HKUST-1 composite: enhancing the CO2 adsorption properties of HKUST-1. *ACS omega* **2019,** *4*, 5275-5282.

42. Prasanth, K. P.; Rallapalli, P.; Raj, M. C.; Bajaj, H. C.; Jasra, R. V., Enhanced hydrogen sorption in single walled carbon nanotube incorporated MIL-101 composite metal–organic framework. *international journal of hydrogen energy* **2011,** *36*, 7594-7601.
43. Li, X.; Zhou, K. F.; Tong, Z. B.; Yang, X. Y.; Chen, C. Y.; Shang, X. H.; Sha, J. Q., Heightened Integration of POM-based Metal–Organic Frameworks with Functionalized Single-Walled Carbon Nanotubes for Superior Energy Storage. *Chemistry–An Asian Journal* **2019,** *14*, 3424-3430.
44. Mao, Y.; Li, G.; Guo, Y.; Li, Z.; Liang, C.; Peng, X.; Lin, Z., Foldable interpenetrated metal-organic frameworks/carbon nanotubes thin film for lithium–sulfur batteries. *Nature communications* **2017,** *8*, 1-8.
45. Ahsan, M. A.; Jabbari, V.; Islam, M. T.; Turley, R. S.; Dominguez, N.; Kim, H.; Castro, E.; Hernandez-Viezcas, J. A.; Curry, M. L.; Lopez, J., Sustainable synthesis and remarkable adsorption capacity of MOF/graphene oxide and MOF/CNT based hybrid nanocomposites for the removal of Bisphenol A from water. *Science of the total environment* **2019,** *673*, 306-317.
46. Jabbari, V.; Veleta, J. M.; Zarei-Chaleshtori, M.; Gardea-Torresdey, J.; Villagrán, D., Green synthesis of magnetic MOF@ GO and MOF@ CNT hybrid nanocomposites with high adsorption capacity towards organic pollutants. *Chemical Engineering Journal* **2016,** *304*, 774-783.
47. Tran, T. Q. N.; Das, G.; Yoon, H. H., Nickel-metal organic framework/MWCNT composite electrode for non-enzymatic urea detection. *Sensors and Actuators B: Chemical* **2017,** *243*, 78-83.
48. Sohrabi, S.; Dehghanpour, S.; Ghalkhani, M., A cobalt porphyrin-based metal organic framework/multi-walled carbon nanotube composite electrocatalyst for oxygen reduction and evolution reactions. *Journal of Materials Science* **2018,** *53*, 3624-3639.
49. Micheroni, D.; Lan, G.; Lin, W., Efficient electrocatalytic proton reduction with carbon nanotube-supported metal–organic frameworks. *Journal of the American Chemical Society* **2018,** *140*, 15591-15595.
50. Jafari, N.; Zeinali, S., Highly Rapid and Sensitive Formaldehyde Detection at Room Temperature Using a ZIF-8/MWCNT Nanocomposite. *ACS omega* **2020,** *5*, 4395-4402.
51. Schulze, H. A.; Hoppe, B.; Schäfer, M.; Warwas, D. P.; Behrens, P., Electrically Conducting Nanocomposites of Carbon Nanotubes and Metal-Organic Frameworks with Strong Interactions between the two Components. *ChemNanoMat* **2019,** *5*, 1159-1169.
52. Lin, R.; Ge, L.; Liu, S.; Rudolph, V.; Zhu, Z., Mixed-matrix membranes with metal–organic framework-decorated CNT fillers for efficient CO2 separation. *ACS applied materials & interfaces* **2015,** *7*, 14750-14757.
53. Yoo, J.; Lee, S.; Lee, C. K.; Kim, C.; Fujigaya, T.; Park, H. J.; Nakashima, N.; Shim, J. K., Homogeneous decoration of zeolitic imidazolate framework-8 (ZIF-8) with core–shell structures on carbon nanotubes. *RSC Advances* **2014,** *4*, 49614-49619.
54. Yang, S. J.; Choi, J. Y.; Chae, H. K.; Cho, J. H.; Nahm, K. S.; Park, C. R., Preparation and enhanced hydrostability and hydrogen storage capacity of CNT@ MOF-5 hybrid composite. *Chemistry of Materials* **2009,** *21*, 1893-1897.
55. Jiang, H.; Feng, Y.; Chen, M.; Wang, Y., Synthesis and hydrogen-storage performance of interpenetrated MOF-5/MWCNTs hybrid composite with high mesoporosity. *International journal of hydrogen energy* **2013,** *38*, 10950-10955.

56. Yang, S. J.; Cho, J. H.; Nahm, K. S.; Park, C. R., Enhanced hydrogen storage capacity of Pt-loaded CNT@ MOF-5 hybrid composites. *International journal of hydrogen energy* **2010,** *35*, 13062-13067.
57. Zhang, Y.; Lin, B.; Sun, Y.; Zhang, X.; Yang, H.; Wang, J., Carbon nanotubes@ metal–organic frameworks as Mn-based symmetrical supercapacitor electrodes for enhanced charge storage. *RSC Advances* **2015,** *5*, 58100-58106.
58. Muschi, M.; Lalitha, A.; Sene, S.; Aureau, D.; Fregnaux, M.; Esteve, I.; Rivier, L.; Ramsahye, N.; Devautour-Vinot, S.; Sicard, C., Formation of a Single-Crystal Aluminum-Based MOF Nanowire with Graphene Oxide Nanoscrolls as Structure-Directing Agents. *Angewandte Chemie* **2020,** *132*, 10439-10444.
59. Bera, K. P.; Haider, G.; Usman, M.; Roy, P. K.; Lin, H. I.; Liao, Y. M.; Inbaraj, C. R. P.; Liou, Y. R.; Kataria, M.; Lu, K. L., Trapped Photons Induced Ultrahigh External Quantum Efficiency and Photoresponsivity in Hybrid Graphene/Metal-Organic Framework Broadband Wearable Photodetectors. *Advanced Functional Materials* **2018,** *28*, 1804802.
60. Li, W. H.; Ding, K.; Tian, H. R.; Yao, M. S.; Nath, B.; Deng, W. H.; Wang, Y.; Xu, G., Conductive metal–organic framework nanowire array electrodes for high-performance solid-state supercapacitors. *Adv. Funct. Mater.* **2017,** *27*, 1702067.
61. Furtado, C. A.; Kim, U. J.; Gutierrez, H. R.; Pan, L.; Dickey, E. C.; Eklund, P. C., Debundling and dissolution of single-walled carbon nanotubes in amide solvents. *J. Am. Chem. Soc.* **2004,** *126*, 6095-105.
62. Sarker, B. K.; Shekhar, S.; Khondaker, S. I., Semiconducting enriched carbon nanotube aligned arrays of tunable density and their electrical transport properties. *ACS Nano* **2011,** *5*, 6297-6305.
63. Dresselhaus, M. S.; Dresselhaus, G.; Saito, R.; Jorio, A., Raman spectroscopy of carbon nanotubes. *Phys. Rep.* **2005,** *409*, 47-99.
64. Sasaki, K.-i.; Saito, R.; Dresselhaus, G.; Dresselhaus, M. S.; Farhat, H.; Kong, J., Chirality-dependent frequency shift of radial breathing mode in metallic carbon nanotubes. *Phys. Rev. B* **2008,** *78*, 235405.
65. Hmadeh, M.; Lu, Z.; Liu, Z.; Gándara, F.; Furukawa, H.; Wan, S.; Augustyn, V.; Chang, R.; Liao, L.; Zhou, F.; Perre, E.; Ozolins, V.; Suenaga, K.; Duan, X.; Dunn, B.; Yamamto, Y.; Terasaki, O.; Yaghi, O. M., New Porous Crystals of Extended Metal-Catecholates. *Chemistry of Materials* **2012,** *24*, 3511-3513.
66. Rubio-Gimenez, V.; Galbiati, M.; Castells-Gil, J.; Almora-Barrios, N.; Navarro-Sanchez, J.; Escorcia-Ariza, G.; Mattera, M.; Arnold, T.; Rawle, J.; Tatay, S.; Coronado, E.; Marti-Gastaldo, C., Bottom-Up Fabrication of Semiconductive Metal-Organic Framework Ultrathin Films. *Adv. Mater.* **2018,** *30*, 1704291.
67. Walton, K. S.; Snurr, R. Q., Applicability of the BET method for determining surface areas of microporous metal-organic frameworks. *J. Am. Chem. Soc.* **2007,** *129*, 8552-6.
68. Chun, K. Y.; Oh, Y.; Rho, J.; Ahn, J. H.; Kim, Y. J.; Choi, H. R.; Baik, S., Highly conductive, printable and stretchable composite films of carbon nanotubes and silver. *Nat. Nanotechnol.* **2010,** *5*, 853-7.
69. Lerner, M. B.; Resczenski, J. M.; Amin, A.; Johnson, R. R.; Goldsmith, J. I.; Johnson, A. T., Toward quantifying the electrostatic transduction mechanism in carbon nanotube molecular sensors. *J. Am. Chem. Soc.* **2012,** *134*, 14318-21.

70. Heller, I.; Chatoor, S.; Mannik, J.; Zevenbergen, M. A.; Dekker, C.; Lemay, S. G., Influence of electrolyte composition on liquid-gated carbon nanotube and graphene transistors. *J. Am. Chem. Soc.* **2010,** *132*, 17149-56.

TOC graphic